# Probing molecular layers with low-energy electrons

Tebyani, A.

# 6

# Band Structure of Few-Monolayer Pentacene Films Above the Vacuum Level

**Abstract**

In the previous chapter, we examined the evolution of unoccupied electronic states above the vacuum level in pentacene films of one to four monolayers in thickness. We then discussed how these states affect secondary electron processes, such as photo-electron and secondary electron emission. These unoccupied states were measured for electrons at normal incidence to and reflection from the sample. In this chapter, we show measurements related to unoccupied states for incident electrons with non-zero in-plane momentum. This allows us to obtain a fuller picture of the unoccupied band structure of pentacene films.

## 6.1 Introduction

In this chapter, we discuss the unoccupied band structure of pentacene films above the vacuum level obtained using Angle-Resolved Reflected Electron Spectroscopy (ARRES). [1,2] We show the results obtained on pentacene films of two and three monolayers in thickness as well as the evolution of pentacene band structure as a result of beam damage, and discuss the features observed in the band structure.

## 6.2 Experimental Technique and Results

Fig. 6.1 shows the diffraction pattern corresponding to the thin film pentacene phase with a herringbone crystal structure. This pattern is obtained on a three-monolayer film. A few of the diffraction spots are annotated in the figure. The first-order spots (indicated by crosses) are not visible at the specific beam energy used for recording this diffraction pattern. The central spot, Γ (Gamma), corresponds to normal incidence and reflection of electrons, i.e. diffraction spot (0,0). In Fig. 6.1, we see also two rectangles. The bigger rectangle, with dashed lines, indicates the Brillouin zone of the pentacene crystal. Any point within this rectangle other than Γ represents electronic states with non-zero in-plane momenta. The smaller rectangle is discussed below.

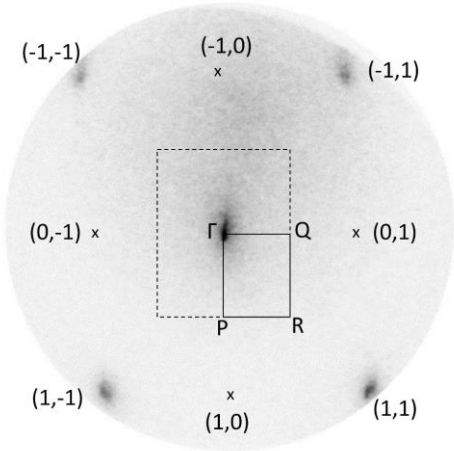


Fig. 6.1 Diffraction pattern of pentacene thin film with a herringbone crystal structure. A few of the diffraction spots are annotated. Γ spot denotes normal incidence and reflection of electrons, i.e. diffraction spot (0,0). Lower-order diffraction peaks are not visible at the beam energy used for recording the pattern. The dashed rectangle denotes the Brillouin zone. The solid rectangle denotes the region of the Brillouin zone imaged at various electron beam intensities (Fig. 6.2). The crosses indicate the position of the 1st-order diffraction peaks, not visible at the beam energy used for imaging the diffraction pattern.

We discussed earlier that we can probe the electronic density of states (DOS) above the vacuum level with LEEM-IV spectra. More precisely, the intensity of reflected electrons as a function of incident beam energy depends on the presence of such states as well as the probability of transmission into such states. The latter can in principle be calculated from the Schrödinger equation. In Fig. 5.2 of the previous chapter, LEEM-IV spectra of one to four monolayer films were shown, obtained by following the intensity variations at Γ, i.e. for normal incidence and reflection. By providing the incident electrons with non-zero in-plane momentum when interacting with the sample, i.e. by tilting the electron beam, we can measure the specular reflectivity (i.e. measure the LEEM-IV spectrum) of other points within the Brillouin zone as well. That is, by scanning the electron beam over (a part of) the Brillouin zone, instead of keeping it fixed at point Γ, we can obtain information about the DOS across the Brillouin zone. Thus, a fuller characterization of the band structure above the vacuum energy becomes possible. This technique is called 'scanning Angle-Resolved Reflected Electron Spectroscopy (ARRES)'. [1,2]

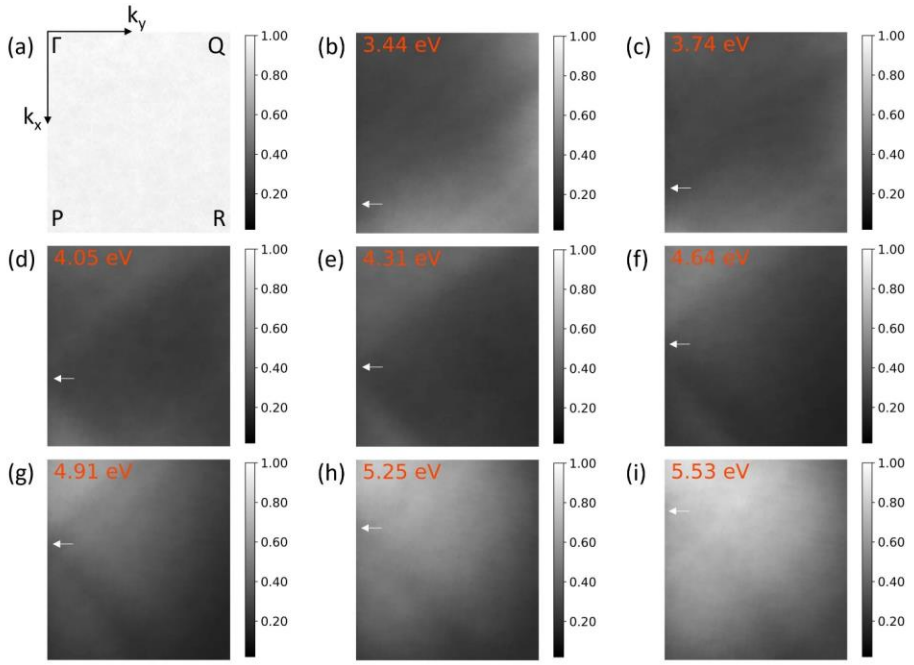


Fig. 6.2 Electron beam reflectivities of the part of pentacene thin film Brillouin zone denoted by the solid rectangle in Fig. 6.1, imaged at various beam energies. The corners of the imaged area annotated as Γ, P, Q and R in (a) correspond to the points in Fig. 6.1. The $k_x$ and $k_y$ axes indicate the directions of the in-plane momenta of the electrons. The Γ spot (top left corner) indicates normal incidence and reflection of electrons, i.e. no in-plane momenta. The white arrows highight the evolution of an electronic state along the $k_x$ axis, i.e its movement towards the Γ spot, as a function of energy. The pentacene film is three monolayers in thickness. The image in (a) is recorded at a beam energy corrsponding to total reflection.

For the results in this chapter, we have measured the reflectivity as a function of position in reciprocal space. More exactly, for the portion of the Brillouin zone indicated by the smaller rectangle in Fig. 6.1, with solid lines and its corners annotated with Γ, P, R and Q. The results at nine different energies are shown in Fig. 6.2. They have been obtained locally on a three-monolayer pentacene film. In Fig. 6.2, each of the images show the reflectivity across the measured part of the Brillouin zone at the indicated energies. The corners of the reflectivity images in Fig. 6.2 (a-i) correspond to points Γ, P, R and Q, as annotated in Fig. 6.2(a). The interpretation of the images is similar to LEEM-IV spectra; existence of electronic states at certain in-plane momenta at a given energy results in a lower reflectivity, while lower DOS and bandgaps will generally result in a higher reflectivity. Given that each reflectivity image contains information about the DOS across (a portion of) the Brillouin zone at a given energy, stacking such reflectivity images obtained for electron energies within a given range, creates a full representation with all possible in-plane momenta across (the measured portion of) the Brillouin zone as a function of energy. In other words, it creates a full mapping related to the unoccupied band structure above the vacuum level. Figure 6.3(a) shows such a stack for the measurement that includes the selection of ARRES images shown in Fig. 6.2. We emphasize that, as mentioned earlier, the reflectivity also depends on the quantum mechanical probability of coupling of both the incident and reflected vacuum electron plane waves to the wavefunction of the available electronic states. The higher this probability, the lower the reflectivity. Furthermore, we note that the DOS measured with 'scanning ARRES' is the projection of the three-dimensional DOS of the sample along the out-of-plane direction ($k_z$).

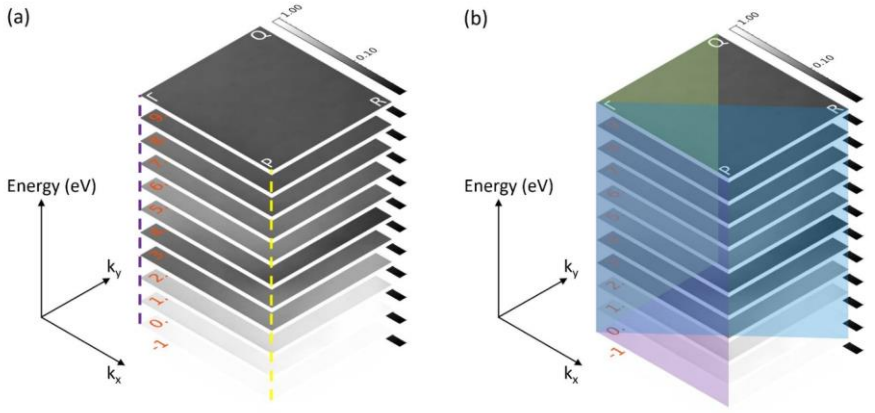


Fig. 6.3 A stack of reflectivity images of part of pentacene thin film Brillouin zone (solid rectangle in Fig. 6.1) imaged within the energy range -1 eV to 10 eV. 0 eV corresponds to the vacuum level. Such a stack visualizes the dependence of the unoccupied DOS on energy and in-plane momentum. The purple and yellow dashed lines in (a) correspond to Fig. 6.4, and show energy-dependence of the unoccupied DOS at various $k_x$ values (with $k_y = 0$). The three planar cuts through the stack in (b) corresponds to Fig. 6.5.

As mentioned before, this 'scanning ARRES' technique is a generalization of LEEM-IV spectroscopy. Fig. 6.3(a) clarifies the relation between the two. Plotting the intensity variations as a function of incident electron energy along the purple dashed line yields the LEEM-IV spectrum at the point Γ, i.e. for normal incidence and reflection of electrons. This curve is shown in Fig. 6.4, with the corresponding color. It is essentially the same as the LEEM-IV curve for a three-monolayer pentacene film shown in Fig. 5.2 in the previous chapter, except that some details of the spectrum are more smeared out. With information about the DOS now available also for states with non-zero in-plane momenta ($k_x$ and $k_y$), we can plot LEEM-IV spectra for any given state with arbitrary $k_x$ and $k_y$. For example, the yellow dashed line in Fig. 6.3(a) corresponds to the LEEM-IV spectrum at point P (see Fig. 6.1). Fig. 6.4 shows LEEM-IV spectra for points Γ and P, as well as three equally-spaced intermediate points between the two. In the figure, the curves are annotated with numbers from 1 (point Γ) to 5 (point P).

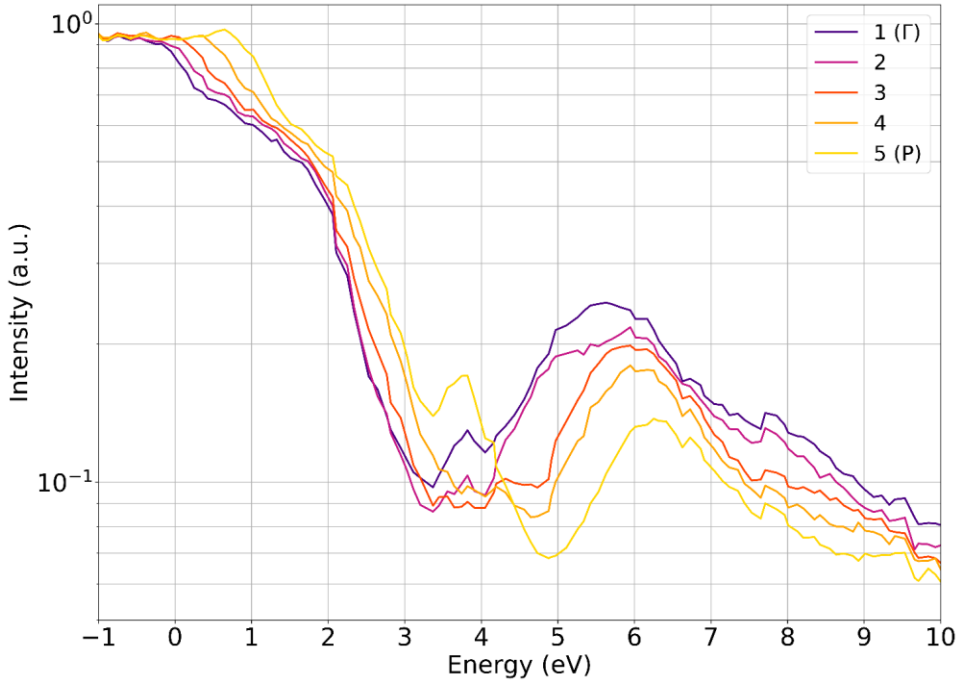


Fig. 6.4 The unoccupied DOS of a pentacene film three monolayers in thickness as a function of energy, obtained at five different points within the Brillouin zone along the Γ-P line in Fig. 6.3.

In addition to LEEM-IV spectra at points corresponding to specific in-plane momenta ($k_x$ and $k_y$), such as those in Fig. 6.4, we can also plot the measured signal across arbitrary lines in the Brillouin zone. Three such lines extend from point Γ to each of the other corners of the rectangle, i.e. points P, Q and R. Fig. 6.3(b) visualizes these linecuts with planes in colors purple, green and blue, corresponding to Γ-P, Γ-Q and Γ-R linecuts, respectively. The results from each of these planes are shown in Fig. 6.5, for a three-monolayer pentacene film. Note that the LEEM-IV spectra in Fig. 6.4 correspond to intensity variations along five equally-spaced (with regards to $k_x$) vertical lines in Fig. 6.5(a). Two of these lines are highlighted (dashed purple and yellow), corresponding to LEEM-IV spectra at points Γ and P, respectively.

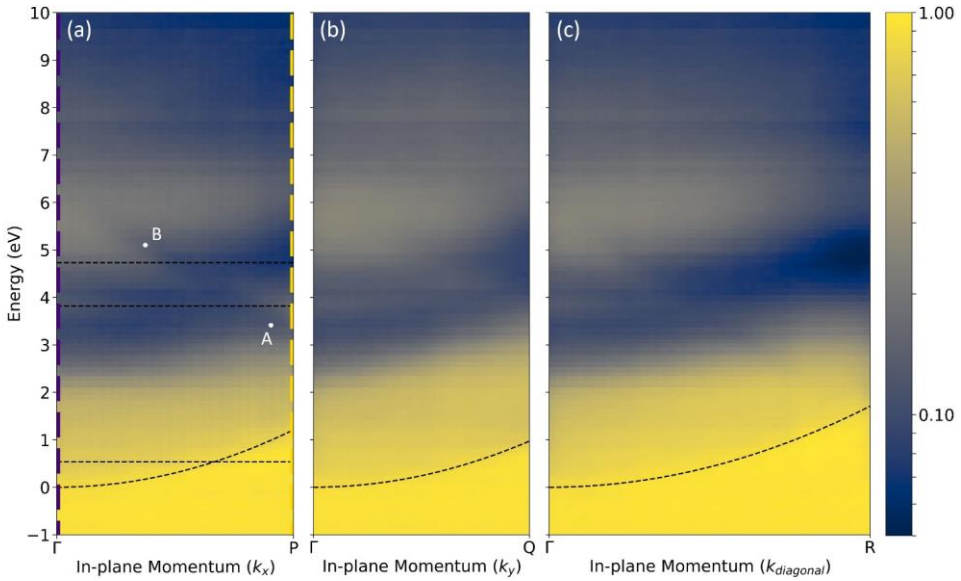


Fig. 6.5 Planar cuts through the stack in Fig. 6.3. Each subfigure shows the dependence of the unoccupied DOS of a three-monolayer pentacene film on both energy and in-plane momentum along three different directions (x, y and diagonal). The purple and yellow dashed lines in (a) correspond to dashed lines of the same colour in Fig. 6.3 and Fig. 6.4. The parabolic black dahsed line in (a), centered at point Γ, is a fit to the derivative of the linecut subfigure along the energy direction. This parabola indicates the mirror-mode transition energy as a function of in-plane momentum. The three horizontal black dashed lines in (a) correspond to Fig. 6.7. Points denoted "A" and "B" in (a) correspond to the evolution of an electronic state as a function of energy and in-plane momentum, also denoted by white arrows in Fig. 6.2.

Linecuts such as those in Fig. 6.5 and series of ARRES reflectivity images at constant energies such as those in Fig. 6.2, help us follow the evolution of electronic states across energy and in-plane momenta. For example, in Fig. 6.5(a) we see the movement of an

electronic state near point P around 3.3 eV toward point Γ as the energy increases, forming a negatively sloped line. The two ends of this line are indicated by white dots called A and B in Fig. 6.5(a). This development can be observed also in Fig. 6.2 by following the position of the small white arrow moving toward Γ with increasing energy.

In all three subfigures of Fig. 6.5, we see black dashed lines with the shape of a parabola centered at point Γ and energy of 0 eV. These parabolas are obtained from parabolic fits to the derivatives of the linecut images in Fig. 6.5 along the energy direction. We discussed previously that in LEEM-IV spectra, negative energies indicate that the incident electrons do not have sufficient kinetic energy to reach the sample, resulting in total reflection. The energy at which the electrons reach the sample with an interaction energy of 0 eV is called the mirror-mode transition (MMT) energy. The electrons with this energy are slowed down to a kinetic energy of 0 eV by the electric field of 10 kV/mm between the grounded objective lens and the sample. Given that the energy of the incident electrons can be written as

$$E = \frac{h^2}{8m\pi^2}\,(k_x^2 + k_y^2 + k_z^2),$$

it is easy to see that if the electrons have non-zero in-plane momenta, a higher kinetic energy is required for $k_z$ (out-of-plane momentum) to be sufficient for the electrons to reach the sample. In other words, the MMT is shifted to higher values if the incident electrons have non-zero in-plane momenta. The schematic in Fig. 6.6 illustrates this point for three electrons with the same energy but different values of in-plane momenta ($k_x$). Here, electrons with larger in-plane momentum are reflected earlier than those with smaller in-plane momentum (and, hence, larger out-of-plane momentum). The shift of the MMT toward higher energies can also be seen in the LEEM-IV spectra in Fig. 6.4, where the spectra obtained at points with higher in-plane momenta (closer to point P) come out of total reflection at higher energies.

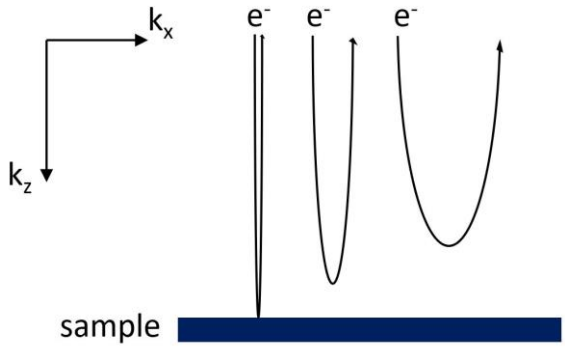


Fig. 6.6 Schematic illustrating the reflection of three electrons with the same energy but different in-plane momentum from the sample. The electrons with larger values of in-plane momentum are reflected earlier. In other words, they require higher energies to reach the sample, leading to the dependence of mirror-mode transition energy on in-plane momentum (see the parabolic dashed line in Fig. 6.5(a)).

In Fig. 6.5, all the points below the parabola correspond to total reflection. This is also observable in Fig. 6.7. Here, we have plotted reflected intensity as a function of in-plane momentum ($k_x$) at several fixed energies, obtained from profiles of the black horizontal dashed lines in Fig. 6.5(a). The line profile obtained at 0.53 eV shows high reflectivity close to point P (larger in-plane momentum and near-total reflection), and lower reflectivity close to point Γ (smaller in-plane momentum). The other two line profiles in Fig. 6.7, obtained at energies 3.82 eV and 4.73 eV show that the specular reflectivity (indicative of DOS) varies as a function of in-plane momentum. In other words, the electronic bands of pentacene films do not appear to be flat (see also Fig. 6.5). This is a surprising finding compared to the reports of relatively flat bands in pentacene at lower energies, such as around the Fermi energy. Photoemission measurements on thin film phase pentacene found a dispersion of only ~190 meV at room temperature [3]. Angle-Resolved Ultraviolet Photoelectron Spectroscopy (ARUPS) measurements on pentacene crystals also show dispersion values below 0.5 eV at room temperature. [4] Similarly, various theoretical calculations of pentacene in thin film and bulk phases show similar dispersion values, all well below 1 eV. [5,6] In contrast, the electronic bands in Fig. 6.5 appear to have a higher degree of dependence of DOS on in-plane momentum. We note the non-flatness of the DOS in Fig. 6.5 is not necessarily indicative of higher dispersion. The regions with higher DOS (lower reflectivity) in Fig. 6.5 can be a superimposition of several bands that are not individually resolved in our measurements. [7] Nonetheless, the band structure of pentacene shows a higher degree of dependence on in-plane momentum above the vacuum level compared to around Fermi energy.

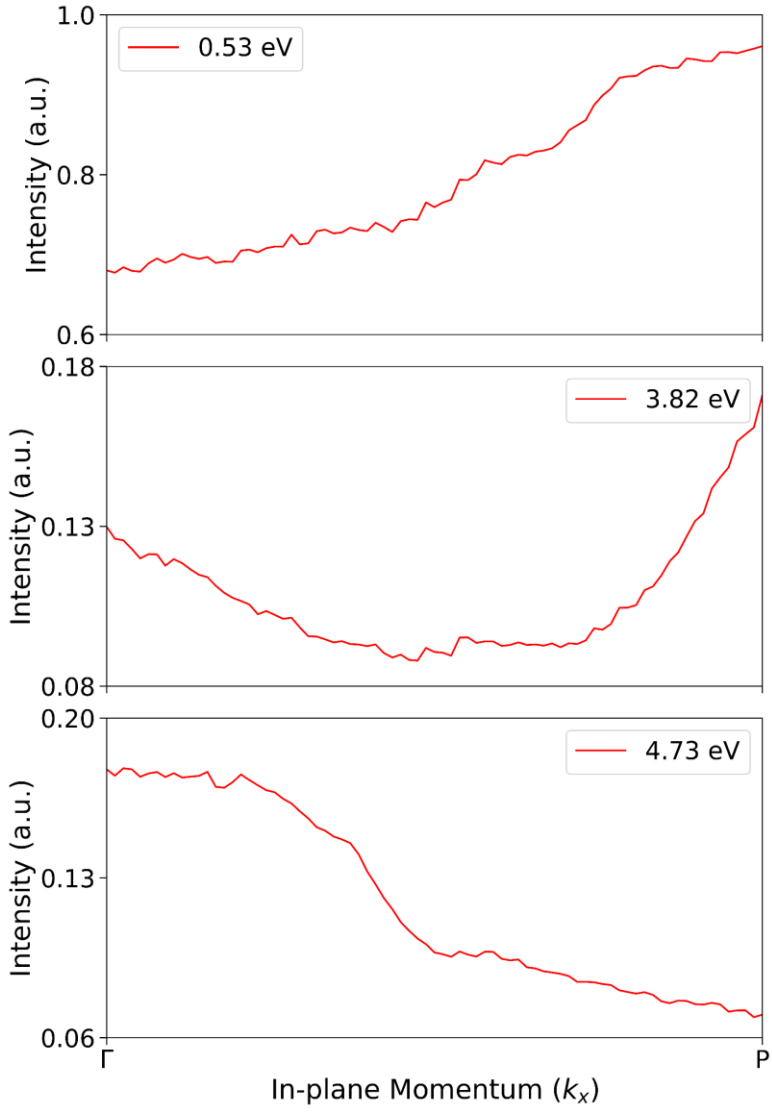


Fig. 6.7 Dependence of the unoccupied DOS of a three-monolayer pentacene film on in-plane momentum ($k_x$), obtained at three different energies of 0.53 eV, 3.82 eV and 4.73 eV above the vacuum level. The linecuts correspond to the horizontal black dashed lines in Fig. 6.5(a).

Furthermore, the width of the electronic bands in Fig. 6.5 appears to be greater than those around the Fermi energy. For example, the apparent width of the high-DOS region centered at 3.5 eV in a LEEM-IV at Γ (see Fig. 6.4) is bigger than 1 eV, while the width of the valence band in pentacene single crystals is a fraction of 1 eV. There are a few possible explanations

for this. Theoretical calculations of pentacene band structure show that the bands near the Fermi level are widely separated/ fairly isolated from each other, while those much below or above the Fermi level are densely packed and overlapping. [8] Hence, the relatively wide bands in Fig. 6.5 can be the superimposition of several unresolved bands. [7] Another possible reason has to do with the molecular orbitals. Bandwidths of electronic bands are very sensitively dependent on the orbital overlap between adjacent molecules (or more generally, elements of a crystal), with more overlap expected to result in wider bands. Generally, higher-energy molecular orbitals are more delocalized. Hence, it is not surprising if the molecular orbitals of the unoccupied states above the vacuum level have stronger interactions with each other, leading to wider bands, and possibly more dispersion at these high energies. A third possible reason is the relatively low lifetime of the electronic states above the vacuum level, experimentally measured and found to vary between a few attoseconds and about 100 attoseconds in Ni(111), Ag(111) and Au(111). [9,10] From the Heisenberg uncertainty principle, a relatively short lifetime for these states results in larger uncertainty about their energies, manifested as larger apparent bandwidths. We note that from our measurements it is not possible to conclude which of these factors is dominant.

In Fig. 6.8, we show similar ARRES linecut measurements obtained on a two-monolayer pentacene film. Fig. 6.9 shows vertical linecuts (i.e. LEEM-IV spectra) at five equally-spaced intervals along $k_x$ direction between the points Γ and P. Interestingly, the general shapes of the features in Fig. 6.8 do not differ much from those observed for the three-monolayer film. The main difference is that the features in the thicker film are more pronounced, as evident from a comparison of Fig. 6.4 and Fig. 6.9. This observation was discussed in the previous chapter, regarding the evolution of the LEEM-IV spectra for specularly-reflected electrons for pentacene films of one to four monolayers in thickness (Fig. 5.2). The fact that the features and dispersions in the two-monolayer film do not differ much from the three-monolayer film can be a result of relatively weak electronic interactions between the layers. In other words, the band structure of the film is probably mostly derived from that of an individual layer.

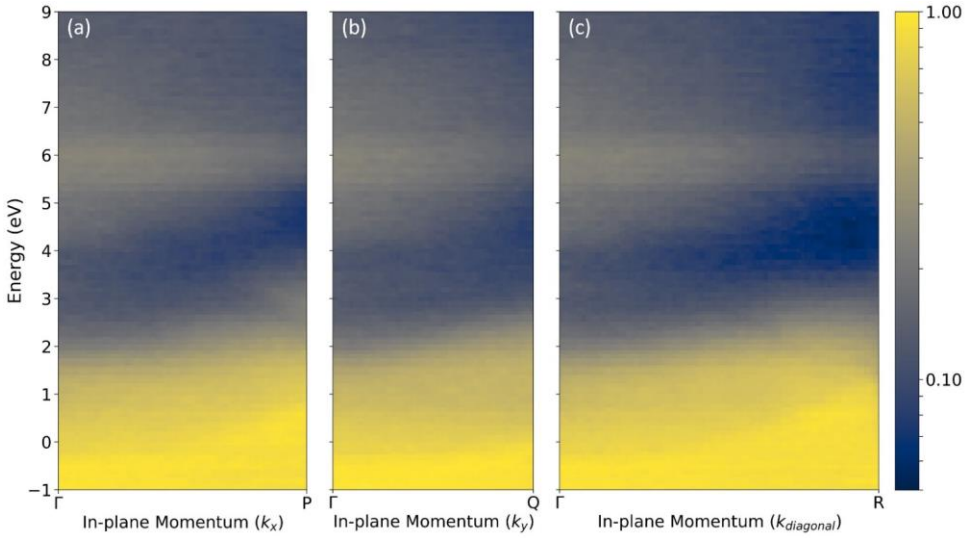


Fig. 6.8 Dependence of the unoccupied DOS of a two-monolayer pentacene film on energy and in-plane momentum along three different directions (x, y and diagonal). The points Γ, P, Q and R correspond to locations of the Brillouin zone indicated in Fig. 6.1. Note that two-monolayer and three-monolayer pentacene thin films have the same crystal structure.

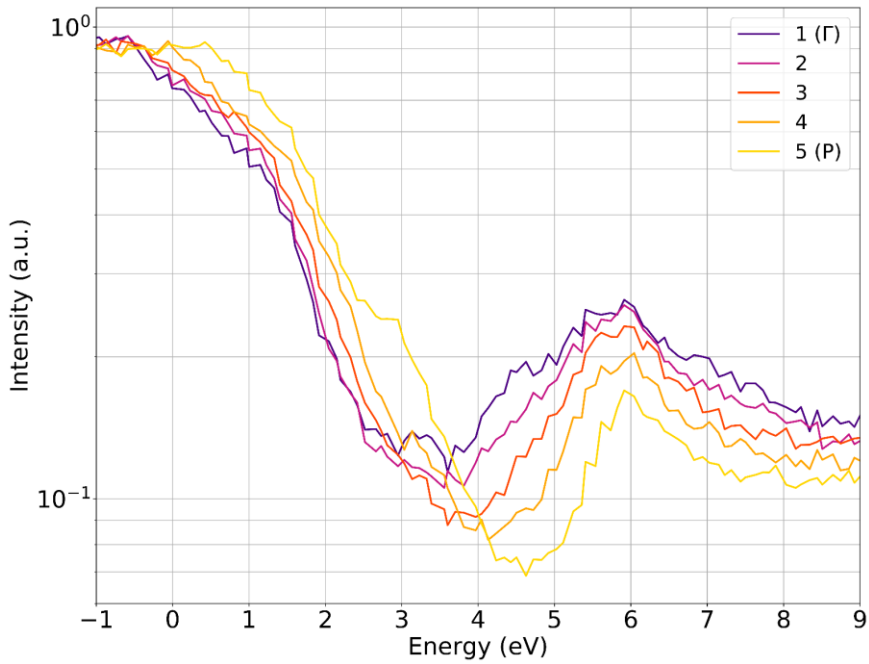


Fig. 6.9 Dependence of the unoccupied DOS of a two-monolayer pentacene film on energy, obtained at five diffferent spots along the Γ-P line (see Fig. 6.3).

In chapter 4, we explored electron beam irradiation damage to pentacene films and discussed the energy dependence of damage cross-section. In Fig. 4.4 of chapter 4, we demonstrated that the features in LEEM-IV spectra gradually diminish upon consecutive measurements on the same area of the sample, as a result of destruction of pentacene crystal lattice. [11] Here we show similar developments in ARRES measurements. Fig. 6.10 illustrates the changes in the Γ-P linecuts in three consecutive ARRES measurements on the same area. The increasing noise for the later measurements is due to the shorter integration time in obtaining the images in order to limit the amount of irradiation damage. Ignoring the noise, we observe lower intensity for the features in the later measurements. This is illustrated in Fig. 6.11, where the three spectra in each subfigure compare the LEEM-IV at Γ (left) and P (right) points between the three measurements. The band structure features in Fig. 6.10 also seem to be smeared out in the later measurements, although the noise makes it difficult to reach a definite conclusion. We also point out that given the diminishingly small damage cross-section found in chapter 4 for electrons up to 5-6 eV, the main features in the ARRES linecut plots for the three-monolayer and two-monolayer films (Fig. 6.5 and Fig. 6.8) are not an artefact of beam damage, and represent genuine characteristics of the DOS (modulated by the efficiency of coupling of the free electron wavefunction to those of the electronic states [12]).

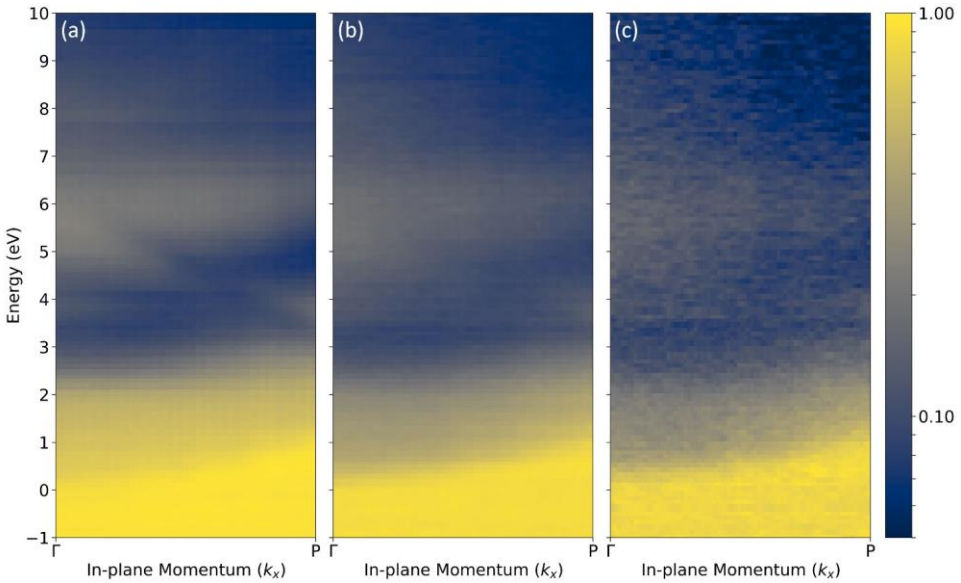


Fig. 6.10 The unoccupied band structure of a three-monolayer pentacene film in three consecutive measurements on the same area. The points Γ and P correspond to those in Fig. 6.1. The decrease in reflected intensity in each subsequent measurement is a result of electron beam irradiation damage. The increasing noise in the later measurements is due to the reduced integration time in obtaining the data.

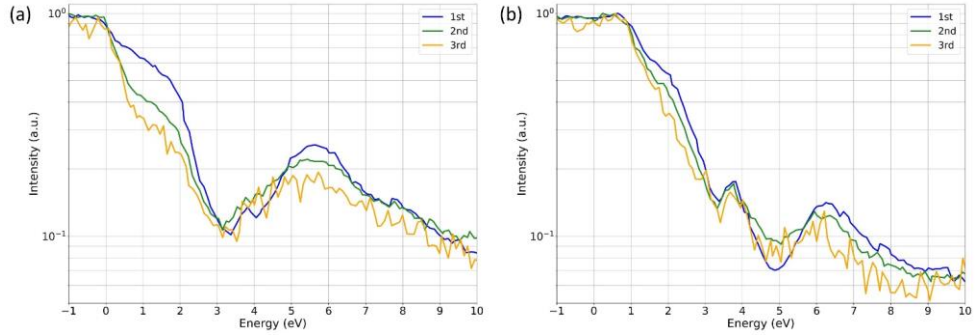


Fig. 6.11 Changes in the unoccupied DOS at points Γ and P, subfigures (a) and (b) respectively, during three consecutive measurements on the same area.

## 6.3 Conclusions

To summarize, we have performed scanning ARRES experiments on three-monolayer and two-monolayer pentacene films. The resulting signal gives direct information about the unoccupied band structure above the vacuum level. The films used are crystalline, in the thin film phase with a herringbone structure. We found a surprising degree of dependence of DOS on in-plane momenta, in contrast to the (nearly-) flat bands reported at energies below the vacuum level. We compared the band structure of three-monolayer and two-monolayer films and found the features to be generally the same on both, but more pronounced on the thicker film, in agreement with our observation of the evolution of LEEM-IV spectra as a function of layer count in the previous chapter. We also discussed the changes in ARRES linecuts as a result of electron beam damage from consecutive measurements on the same area. We found similar developments to those observed in chapter 4 for LEEM-IV spectra, i.e. diminishing of features due to damage to the pentacene film.

In the previous chapter, we discussed the critical role of unoccupied electronic states above the vacuum level, acting as ‘intermediate’ states, in photo-electron and secondary electron emission. Here, we demonstrated, for pentacene films, the dependence of these intermediate states on in-plane momentum. Our results, combined with information about the in-plane dispersion of the occupied ‘initial’ states, provide a fuller picture for the analysis of secondary electron processes, i.e. photo-electron and secondary electron emission, in pentacene films.

## References

[1] J. Jobst, A. J. H. van der Torren, E. E. Krasovskii, J. Balgley, C. R. Dean, R. M. Tromp, and S. J. van der Molen, *Quantifying Electronic Band Interactions in van der Waals Materials Using Angle-Resolved Reflected-Electron Spectroscopy*, Nat. Commun. **7**, 13621 (2016).

[2] J. Jobst, J. Kautz, D. Geelen, R. M. Tromp, and S. J. van der Molen, *Nanoscale Measurements of Unoccupied Band Dispersion in Few-Layer Graphene*, Nat. Commun. **6**, 8926 (2015).

[3] N. Koch, A. Vollmer, I. Salzmann, B. Nickel, H. Weiss, and J. P. Rabe, *Evidence for Temperature-Dependent Electron Band Dispersion in Pentacene*, Phys. Rev. Lett. **96**, 156803 (2006).

[4] Y. Nakayama, Y. Mizuno, M. Hikasa, M. Yamamoto, M. Matsunami, S. Ideta, K. Tanaka, H. Ishii, and N. Ueno, *Single-Crystal Pentacene Valence-Band Dispersion and Its Temperature Dependence*, J. Phys. Chem. Lett. **8**, 1259 (2017).

[5] M. L. Tiago, S. G. Louie, M. L. Tiago, S. G. Louie, and J. E. Northrup, *Ab Initio Calculation of the Electronic and Optical Properties of Solid Pentacene*, Phys. Rev. B **67**, 115212 (2003).

[6] D. Nabok, P. Puschnig, C. Ambrosch-Draxl, O. Werzer, R. Resel, and D. M. Smilgies, *Crystal and Electronic Structures of Pentacene Thin Films from Grazing-Incidence x-Ray Diffraction and First-Principles Calculations*, Phys. Rev. B **76**, 235322 (2007).

[7] Björn Baumeier, *Private Communication*.

[8] X. Leng, J. Feng, T. Chen, C. Liu, and Y. Ma, *Optical Properties of Acene Molecules and Pentacene Crystal from the Many-Body Green's Function Method*, Phys. Chem. Chem. Phys. **18**, 30777 (2016).

[9] Zhensheng Tao, Cong Chen, Tibor Szilvási, Mark Keller, Manos Mavrikakis, Henry Kapteyn, and Margaret Murnane, *Direct Time-Domain Observation of Attosecond Final-State Lifetimes in Photoemission from Solids*, Science **353**, 62 (2016).

[10] R. Locher, L. Castiglioni, M. Lucchini, M. Greif, L. Gallmann, J. Osterwalder, M. Hengsberger, and U. Keller, *Energy-Dependent Photoemission Delays from Noble Metal Surfaces by Attosecond Interferometry*, Optica **2**, 405 (2015).

[11] A. Tebyani, F. B. Baalbergen, R. M. Tromp, and S. J. van der Molen, *Low-Energy Electron Irradiation Damage in Few-Monolayer Pentacene Films*, J. Phys. Chem. C **125**, 26150 (2021).

[12] J. I. Flege and E. E. Krasovskii, *Intensity-Voltage Low-Energy Electron Microscopy for Functional Materials Characterization*, Phys. Status Solidi RRL **8**, 463 (2014).